Engineering Structures 304 (2024) 117601

Contents lists available at ScienceDirect

Engineering Structures

journal homepage: www.elsevier.com/locate/engstruct

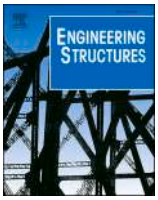

Glass Fiber Reinforced Concrete jointless slabs-on-grade: A real-scale experimental study

Antonio Mudadu [a], Giuseppe Tiberti [a,*], Bryan Barragan [b], Philipp Löber [c], Stephan Friedemann [b], Klaus Holschemacher [c], Giovanni A. Plizzari [a]

[a] Department of Civil, Environmental, Architectural Engineering and Mathematics, University of Brescia, Italy
[b] Concrete Solutions, Owens Corning, Chambéry, France
[c] University of Applied Sciences, Leipzig, Germany

ARTICLE INFO

Keywords:
Glass Fiber Reinforced Concrete
Jointless slabs-on-grade
Shrinkage phenomena
Thermal-effects
Curling

ABSTRACT

The paper presents a real-scale experimental study of Glass Fiber Reinforced Concrete (Glass-FRC) jointless slabs-on-grade in outdoor conditions before the application of service loads to evaluate deformations due to shrinkage phenomena and thermal effects.

A square slab (20 ×20×0.18 m) and a unidimensional slab (2 ×20×0.18 m) reinforced with 10 kg/m^3 of glass macro-fibers were cast and monitored for about six months through external and embedded sensors to detect in-plane and out-plane slab displacements. A double plastic sheet layer was used under the slab to reduce friction with the support while another plastic sheet was applied on the top slab for a curing-time of seven days to reduce risk of cracking. Among the complementary tests, the frictional behavior between the slab and the support was assessed through a large-scale interface shear test. Environmental temperature and relative humidity were continuously measured over the whole period as well as Glass-FRC main mechanical properties. No cracks were detected by visual inspection after approximately six months.

1. Introduction

Industrial floors consist of thin slabs on a continuous subgrade generally defined as slabs-on-grade, whose design guidelines are nowadays available from different organizations [1–4]. Although slabs-on-grade are elements present in structural books [5], in many countries they are still considered as non-structural or secondary structures.

Industrial floors are increasingly made of Fiber Reinforced Concrete (FRC), where randomly and homogeneously distributed fibers allow to reduce or replace conventional reinforcement and to avoid critical phases of the floor construction process [6–9]. Fibers also allow to enhance crack control during the whole service life of the structure [10–14] and significantly enhance fatigue resistance of concrete [15,16], which is particularly important for industrial floors where cyclic loads are generally present. Hence, the use of FRC can lead to enhanced quality floors achieved with higher productivity, simpler execution, and better working environments.

Glass macro-fibers have been successfully used in many countries around the world as primary reinforcement for slabs-on-grade. The significant post-cracking strength provided by glass macro-fibers for small crack openings is particularly efficient for structures (as slabs on grade) with a high degree of redundancy [17,18], both at Serviceability Limit State (SLS, due to shrinkage phenomena) and Ultimate Limit State (ULS).

The advantages of FRC slabs are even more evident in “jointless” slabs-on-grade (i.e. floors without contraction joints that require lower maintenance costs), where the risk for cracking due to thermal and shrinkage effects is significantly higher and, due to the larger exposed surface without contraction joints, the curling deformations are greatly amplified.

The curling upward deformation is mainly related to the shrinkage gradient along the slab depth, since the surface of the slab shrinks differently than the bottom [19–22]. In slabs on grade curling is mainly controlled by contraction joints (usually saw-cut), whose distance depends on the slab thickness; curling control is more difficult in jointless slabs where contraction joints are not present. Hence, curling of concrete slabs-on-grade remains a major concern and its mitigation is critical for crack control, durability, and structural capacity [23–26].

* Corresponding author. Fax: +39 0303711312
E-mail address: giuseppe.tiberti@unibs.it (G. Tiberti).

https://doi.org/10.1016/j.engstruct.2024.117601
Received 11 October 2023; Received in revised form 3 January 2024; Accepted 30 January 2024
Available online 15 February 2024

Nomenclature

E_c	concrete elastic modulus
f_{cm}	mean cylindrical compressive concrete strength
$f_{cm,cube}$	mean cubic compressive concrete strength
f_{ctm}	mean tensile concrete strength
$f_{ctm,spl}$	mean tensile splitting concrete strength
f_{Rim}	mean residual flexural tensile strength of fiber reinforced concrete corresponding to Crack Mouth Opening Displacement, CMOD=$CMOD_i$
f_{uf}	fiber filament tensile strength
L_f	fiber length
L_f/ϕ_f	fiber aspect ratio
ϕ_f	fiber diameter
τ_0	shear frictional stresses between subgrade and slab (end of elastic branch of bilinear function adopted)
δ_0	relative displacement between subgrade and slab (end of elastic branch of bilinear function adopted)

Shrinkage effects could be mitigated by post-tensioning the slabs [27,28] or by incorporating shrinkage-reducing admixtures in the concrete mix; the former solutions increase the complexity of the construction process while the latter solution increases the concrete costs.

It should also be considered that cracking in slabs on grade is significantly influenced by the restraining effects of the slab-to-ground friction [29], which becomes also more significant in jointless slabs due to the absence of contraction joints. Therefore, for a proper slab design, it is worth studying the local interfacial frictional behavior between slab and subgrade, even considering the limited information available into the literature [30,31].

Despite several studies focused on FRC elevated slabs [10,12-14,32] there are very few information on the experimental behavior of real scale slabs on grade in real environmental conditions. In fact, a distinction has to be made between full-scale slabs tests in laboratory conditions and real-slabs tests in real environmental conditions. Referring to the former, that usually have a square size with a side of few meters (3−4), some results are available on the mechanical response [6–9,17] and on the shrinkage response [18,33]. Referring to real-scale slabs in real environmental conditions, having a typical size of a portion of the floor within construction joints (20–30 m), to the best of the Authors knowledge no experimental results are available in the literature so far.

Within this framework, to better evaluate the influence of glass macro-fibers on shrinkage and thermal phenomena, a real-scale experimental study of a Glass Fiber Reinforced Concrete (Glass-FRC) jointless slab-on-grade in outdoor conditions was carried out. A heavily instrumented 20 × 20×0.18 m jointless slab was cast and monitored during more than 6 months (07–2017 to 01–2018), before entering in service. Several external and embedded sensors were implemented to measure in-plane and out-plane slab displacements.

In addition, a 20 m long unidimensional slab with the same thickness as the large jointless slab and similar instrumentation was also cast and monitored during the same period. Environmental temperature and relative humidity were continuously measured over the whole period. The evolution of the main mechanical properties of the Glass FRC along time was also evaluated. The curling phenomena were continuously measured through the whole experimental time.

This real-scale experimental study on slabs on grade is one of the few (and probably the first) experimental tests available that aims to contribute for a better understanding of the behavior of FRC jointless floors. The experimental results allow for a better validation of numerical models to analyze jointless slabs-on-grade, leading to more rational (and sustainable) design procedure. Moreover, in order to better understand the development of interfacial friction stresses and slippage at the slab-subgrade interface, large-scale interface shear tests were carried out on three square slab specimens (1 m side).

The experimental program is presented in Section 2 while main Glass-FRC mechanical properties and development (in-time) of environmental conditions are reported in Sections 3 and 4, respectively. The instrumentation adopted is described (Section 5) while the discussion of main results and trends is presented in Section 6; the main concluding remarks are summarized in Section 7.

2. Experimental program

The behavior of slabs-on-grade under outdoor environmental conditions before the application of service loads depends on slab geometry, subgrade properties, initial curing, material properties and environmental conditions.

Based on a preliminary parametric numerical study [18], the following slabs-on-grade geometries were considered:

- a square slab having a side of 20 m and a thickness of 0.18 m to reproduce a real-scale jointless pavement (Fig. 1a);
- a unidimensional slab 20 m long x 2 m wide x 0.18 m thick (Fig. 1b) to obtain experimental results more readable and comparable with analytical models presented on literature [23,24].

A double plastic sheet layer was placed on the subgrade before casting slabs (Fig. 1b) to considerably reduce the slab-to-subgrade friction which increases the risk of cracking for the slabs [18]. Because of the lack of data available into the literature, in order to better evaluate the slab-to-subgrade friction, three 1 × 1×0.18 m small square samples were included in the experimental program. In fact, this local frictional behavior can be better described by means of a proper stress-slip relationship [30,31], which governs the phenomena from a kinematic point of view.

A concrete strength class C30/37 was adopted, which is representative of slabs-on-grade for concrete floors. Concrete was reinforced with 10 kg/m^3 of glass macro-fibers (Glass-FRC) having a length (L_f) of 36 mm, a diameter (ϕ_f) of 0.54 mm and an aspect ratio (L_f/ϕ_f) equal to 67. These fibers are high-performance alkali-resistant glass macro-fibers with a filament tensile strength (f_{uf}) higher than 1700 MPa and an elastic modulus of 72 GPa (Fig. 2).

Slabs were cast in one of the sites of construction company OTTO HEIL GmbH & Co. KG (Fig. 1a) and they remained in outdoor conditions from July 13rd, 2017 to January15th, 2018 in Leipzig, corresponding to a monitoring-time of about 186 days.

The slabs formworks were filled by means of a truck-mounted concrete pump. Minor compaction was manually applied with a ruler on the

(a) (b)

Fig. 1. Square slab after casting (a) and double plastic sheet layer of unidimensional slab before casting (b).

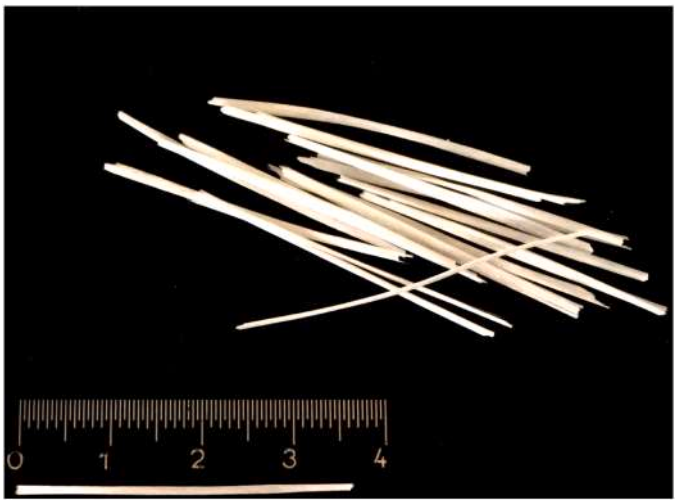

Fig. 2. Glass macro-fibers used.

top of the slab, which was finally troweled to achieve a smooth finishing. As mentioned above, an initial curing time of seven days was adopted [18].

The following samples were cast, together with the slabs, for material characterization (for more details, see Section 3):

- concrete cubes having 0.15 m side for measuring the compressive and splitting tensile concrete strengths according to EN 12390-3 [34] and EN 12390-6 [35], respectively;
- beams $0.15 \times 0.15 \times 0.55$ m for determining Glass-FRC post-cracking properties according to EN 14651 [36];
- prismatic elements $0.10 \times 0.06 \times 1.0$ m for free shrinkage measurement according to EN 12390-16 [37].

Eight batches were necessary for casting unidimensional and square slabs in addition to samples for material characterization (Section 3) and specimens for the evaluation of interfacial friction between slab and subgrade (Section 4). Table 1 lists, for each batch: the casting time, the environmental condition (at the time of casting) and the measures retrieved from flow table tests according to standard [38]. The geometry and the number of standard specimens is reported as well. The test and monitoring programs of these samples are reported in more details in Sections 3 and 4.

3. Material characterization

The concrete properties were investigated as well as the frictional behavior between slabs' bottom surface and subgrade with the interposed double plastic sheet layer.

3.1. Glass-FRC properties

For the mechanical characterization of Glass-FRC, tests summarized in Table 2 were carried out. It should be mentioned that most of the specimens were cured in the same environmental condition of the slabs (defined as "on-site" in Table 2), while some samples were cured in standard conditions (moist room with a relative humidity $> 95\%$; $T = 20 \pm 2\ ^{\circ}C$) until 24 h before being tested at 28 days. In Table 3 compressive and splitting tensile strengths, as determined from on-site cubic samples (outdoor conditions), are reported together with the corresponding Coefficient of Variations (CoVs, in round brackets). In case of compressive strength CoVs are in a typical range while they are slightly higher in splitting tensile strength.

Fig. 3a shows mean compressive concrete strength ($f_{cm,cube}$) evolution along time as retrieved from data collected in Table 3. For each testing time, generally two cubes were tested according to EN 12390–3 [34]. The average concrete compressive strength ($f_{cm,cube}$) at 28 days were 43.9 MPa (CoV: 0.02) and 41.5 MPa (CoV: 0.02) under standard (red dot) and outdoor conditions, respectively. In the latter case, an increase of compressive strength at 140 days was observed (up to 52.7 MPa, about 25% more than that at 28 days). Note that, due to the evolution of temperature and relative humidity, it is not possible to compare the data reported in Fig. 3a with a curve retrieved through typical relationships based on standard constant environmental conditions (relative humidity $> 95\%$; $T = 20 \pm 2\ ^{\circ}C$). Accordingly, a possible logarithmic best-fitting curve with its coefficient of determination is proposed herein.

As summarized in Table 2, 38 cubes were tested according to EN 12390–3 [34], while 35 cubes were tested for measuring the splitting tensile strength ($f_{ctm,spl}$) according to EN 12390–6 [35]. As suggested in current Eurocode 2 [39] (Section 3.1.2, Eq. 3.3), the uniaxial mean tensile concrete strength (f_{ctm}) can be evaluated as $0.9 \times f_{ctm,spl}$.

Fig. 3b shows the mean tensile concrete strength (f_{ctm}) evolution along time: f_{ctm} at 28 days were 2.57 MPa (CoV: 0.06) and 2.55 MPa (CoV: 0.09) under standard (red dot) and outdoor conditions, respectively. In the latter case, the complete time development evidences an increase of strength at 112 days up 3.60 MPa, about 40% than that at 28 days. A prediction of f_{ctm} time development can be done (solid line in Fig. 3b) by taking advantage from relationships proposed in Section 3.1.3 of Eurocode 2 [39] based on $f_{cm,cube}$, which is described by the logarithmic relationship reported in Fig. 3a. It can be noticed a good agreement with experimental data. Similarly, the evolution along time of concrete elastic modulus (E_c) can be calculated, as reported in Fig. 3c. The latter is an important input parameter for a simplified analytical procedure for better understanding the behavior of unidimensional slab, as described in Section 6.

Eleven small beam specimens (Table 1) were tested according to EN 14651 [36] to measure the post-cracking strength of Glass-FRC: two samples were cured in standard conditions to be tested at 28 days, while nine samples were subjected to the same environmental conditions of the slabs and tested at 3, 7 and 28 days (Table 2).

Table 1
Test program for material characterization.

Casting time	Batch	Weather	Temperature		Flow test	Cubes	Beams	Shrinkage
			Air [°C]	Concrete [°C]	[cm x cm]			
8:30 AM	F4	Sun/clouds	18	-	59 × 60	6	1	
9:10 AM	F6	Clouds	18	24	34 × 34	6	1	1
10:00 AM	F7	Sun/clouds	20.7	26	58 × 57	6	2	2
10:30 AM	F8	Clouds	21.4	26.8	55 × 51	9	2	
11:30 AM	F11	Clouds	22.4	-	53 × 51	10	2	
12:10 PM	F12	Clouds	22	-	-	3		
1:20 PM	F13	Rain	26	-	61 × 59	16	2	
1:50 PM	F14	Strong Rain	18	23	-	17	1	2
Total						**73**	**11**	**5**

Table 2
Tests plan for Glass-FRC strength development. The sampling frequency per week is evidenced together with the number of samples tested per week.

Time	Sampling Frequency/week	Compressive strength		Splitting tensile strength		3PBTs (Three Points Bending Tests) EN14651[36]	
		On-site	Standard conditions	On-site	Standard conditions	On-site	Standard conditions
1st week	7x	14		14		6 (3 days, 7 days)	
2nd week	3x	6		6			
3rd week	2x	4		4			
4th week	1x	2	3	2	3	3	2
5th week to 20th week	4x	9		6			
Total		**38**		**35**		**11**	

Table 3
Compressive and splitting tensile strengths of cubic samples in outdoor conditions (CoV in brackets).

Time		f_c	$f_{c,\ mean}$	$f_{ct,sp}$	$f_{ct,sp,mean}$
Week	days	[MPa]	[MPa]	[MPa]	[MPa]
1	1	4.4	4.7	0.44	0.49
		5.0	(0.1)	0.53	(0.13)
	2	12.1	12.1	1.08	1.11
		12.1	(0)	1.13	(0.03)
	3	15.0	14.4	1.37	1.35
		13.8	(0.06)	1.32	(0.03)
	4	19.2	18.7	1.54	1.47
		18.1	(0.04)	1.40	(0.07)
	5	19.4	19.4	1.28	1.39
		19.3	(0)	1.49	(0.11)
	6	22.7	22.9	1.74	1.68
		23.2	(0.01)	1.61	(0.05)
	7	27.8	28.7	2.07	1.98
		29.7	(0.05)	1.89	(0.06)
2	9	27.6	28	2.08	2.11
		28.4	(0.02)	2.14	(0.02)
	12	33.8	33.6	2.22	2.28
		33.4	(0.01)	2.33	(0.03)
	14	36.4	34	2.55	2.69
		31.7	(0.1)	2.82	(0.07)
3	16	33.3	35.1	3.70	3.8
		36.9	(0.07)	3.89	(0.04)
	19	33.0	33.6	1.84	1.99
		34.2	(0.03)	2.14	(0.11)
4	28	41.0	41.5	3.01	2.83
		42.0	(0.02)	2.64	(0.09)
8	56	46.5	47.5	3.31	3.24
		48.6	(0.03)	3.17	(0.03)
12	84	46.2	45.7	2.78	3
		45.3	(0.01)	3.22	(0.1)
16	112	52.8	50.8	4.59	4.01
		48.9	(0.05)	3.42	(0.21)
20	140	52.8	52.7		
		47.7	(0.09)		
		57.6			

In Fig. 4, the mean experimental curves of nominal residual stress vs. Crack Mouth Opening Displacement (CMOD) are plotted at 3, 7, 28 days for samples having on-site curing, together with that at 28 days in standard conditions; the scatter is depicted as well. It can be noticed that there is an unexpected higher post-cracking strengths at 7 days probably due to a higher number of fibers crossing the cracked section (at notch); after 3 days from casting, residual strengths f_{R1m} and f_{R3m} are already 75% to those at 28 days allowing to infer that the glass macro-fiber reinforcement under study may be an efficient solution also to control early age cracking.

Besides the mechanical properties of Glass-FRC previously discussed, the free shrinkage behavior of concrete was also monitored for about 112 days by means of five samples (Table 1). In particular, two prisms (0.10×0.06×1.0 m, Section 2) were subjected to the same environmental conditions of the slabs (free shrinkage prisms were kept next to the slabs). Unfortunately, the results obtained from one of two specimens in outdoor conditions were not reliable and, consequently, not considered. The remaining three samples were subjected to standard condition tests.

Fig. 5a and b show the concrete shrinkage development vs. time for prisms under on site and standard conditions, respectively. In Fig. 5a the seven-days slabs-curing is clear with variation of measurements around small values due to the effect of limited autogenous shrinkage, with only a low expansion probably caused by rainy conditions. After slabs-curing, the deformation increases up to an asymptotic value of about 175 microstrain at 80 days. Measurements retrieved by prisms under standard conditions are characterized by a low dispersion as proven by the mean experimental curve plotted in Fig. 5b; a maximum free shrinkage deformation of about 267 microstrain was measured at 112 days, which is in the expected level for the concrete class used in these tests. The maximum shrinkage deformation exhibited by samples under standard conditions (Fig. 5b) is almost 1.5 times higher than those in on-site environment (Fig. 5a), because in the former the temperature and the relative humidity are controlled ($T = 20 \pm 2\ ^\circ C$ and $RH > 95\%$, respectively), while on-site the environmental temperature decreases in 150 days of about 30 °C (see Section 4) and the relative humidity was higher due to rain during the testing time.

3.2. Interfacial friction between slab and subgrade

In order to better study the internal stresses developing in slabs as result of shortening or elongation in presence of shrinkage or thermal effects, it is necessary to define a proper shear stress-slippage static friction relationship (kinematic law) [18]. The latter governs the capacity of interfacial layer between slab and subgrade and the induced stresses in the slab. Beside the loads, other stresses present in slabs under outdoor conditions are due to flexural induced behavior by curling. A number of experimental studies [30,31] have stated that the relationship between the interfacial friction stresses and slippage at the base of the slab can be described by a bilinear function. The following subgrade-scenarios were investigated [30,31]: flexible granular, natural clay and cement based materials but no information were provided in case of double plastic sheet layer, which is the typical and practical condition often occurring in practice.

To gain new insights into this common interface, three square slab specimens (Fig. 6a) were tested under horizontal load (Fig. 6b) to experimentally obtain the aforementioned kinematic law. Specimens had the same thickness of slabs tested and one square meter surface (Fig. 7a) and were cast on the same subgrade adopted for full-scale slabs, consisting of compacted gravel with an upper layer of compacted fine sand. Before casting concrete, a double plastic sheet layer was placed.

A displacement transducer was mounted on the opposite slab surface aligned to the slippage axis (Fig. 7a). Slab slippage was imposed by means of the hydraulic jack (contrasted by a steel beam, which was anchored with an excavator, Fig. 6c) and measured by the transducer [40].

Fig. 7b shows the experimental curves of shear stress (derived from

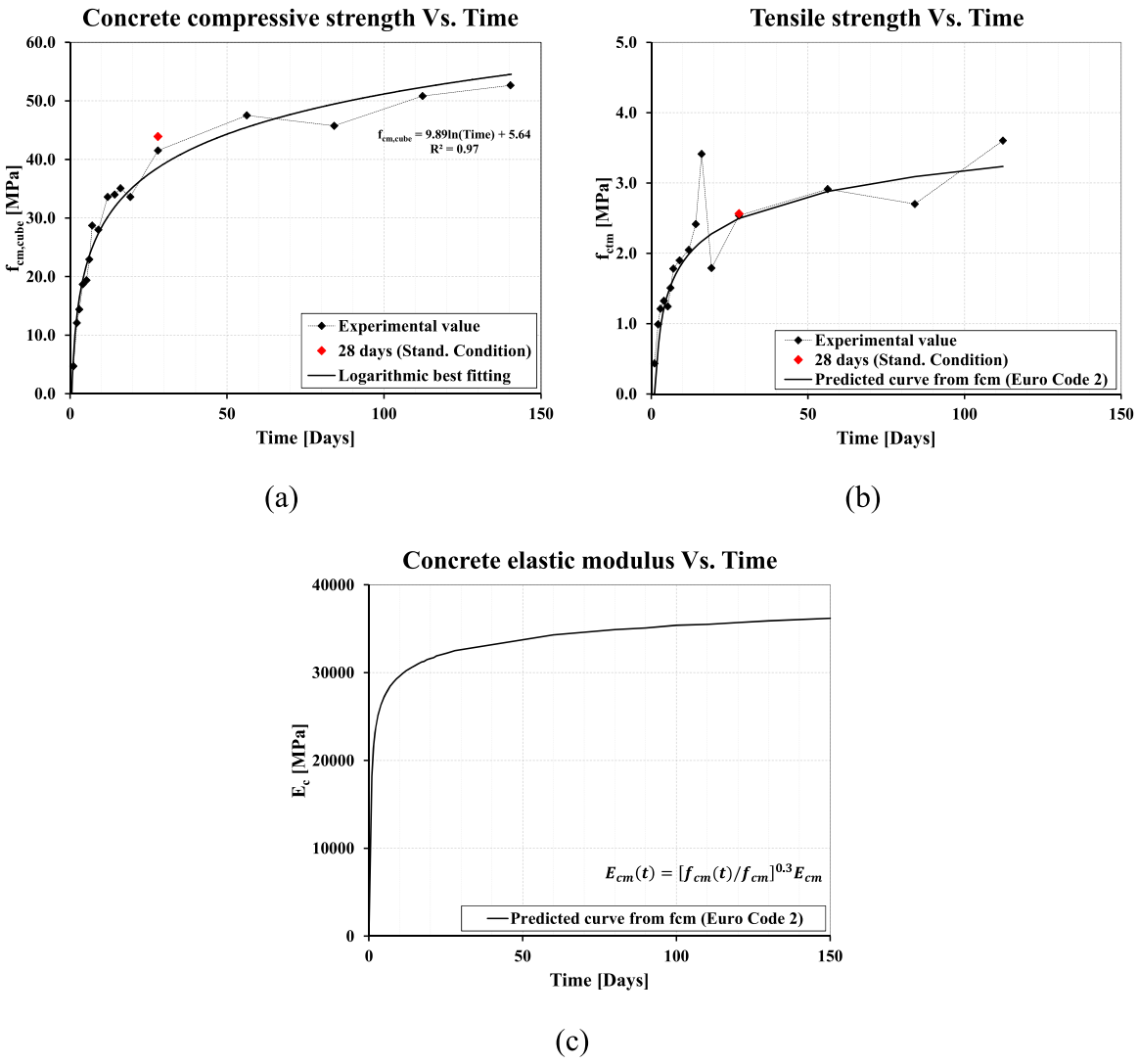

Fig. 3. Compressive (a) and Tensile concrete strength (b) vs. Time based on cubes 150 × 150 × 150 mm^3; Concrete elastic modulus (retrieved by f_c according to Euro Code 2 [39]) evolution vs. Time (c).

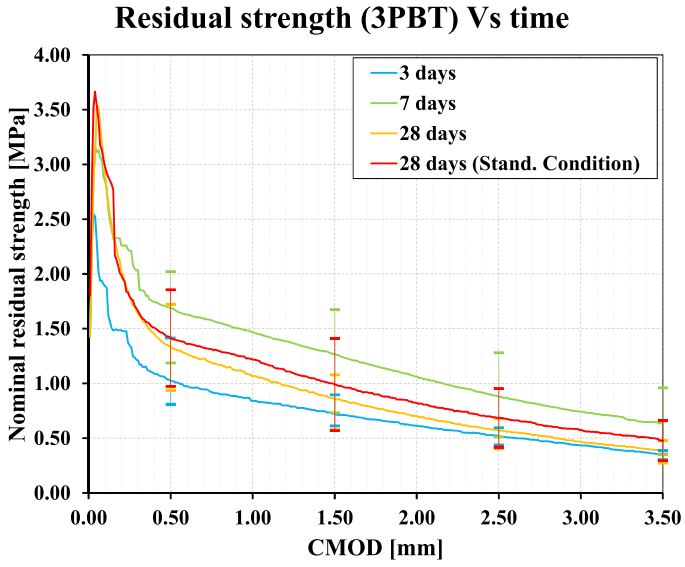

Fig. 4. Nominal stress vs. CMOD mean experimental curves of notched beams with evidenced the scatter at 3, 7, 28 days.

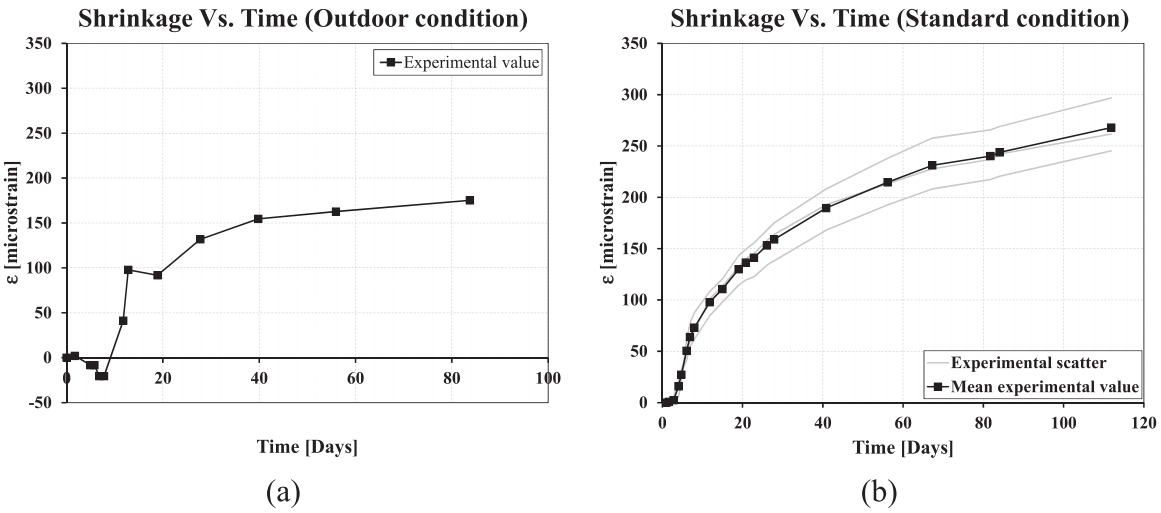

Fig. 5. Concrete shrinkage evolution vs. Time: (a) outdoor condition, (b) standard condition.

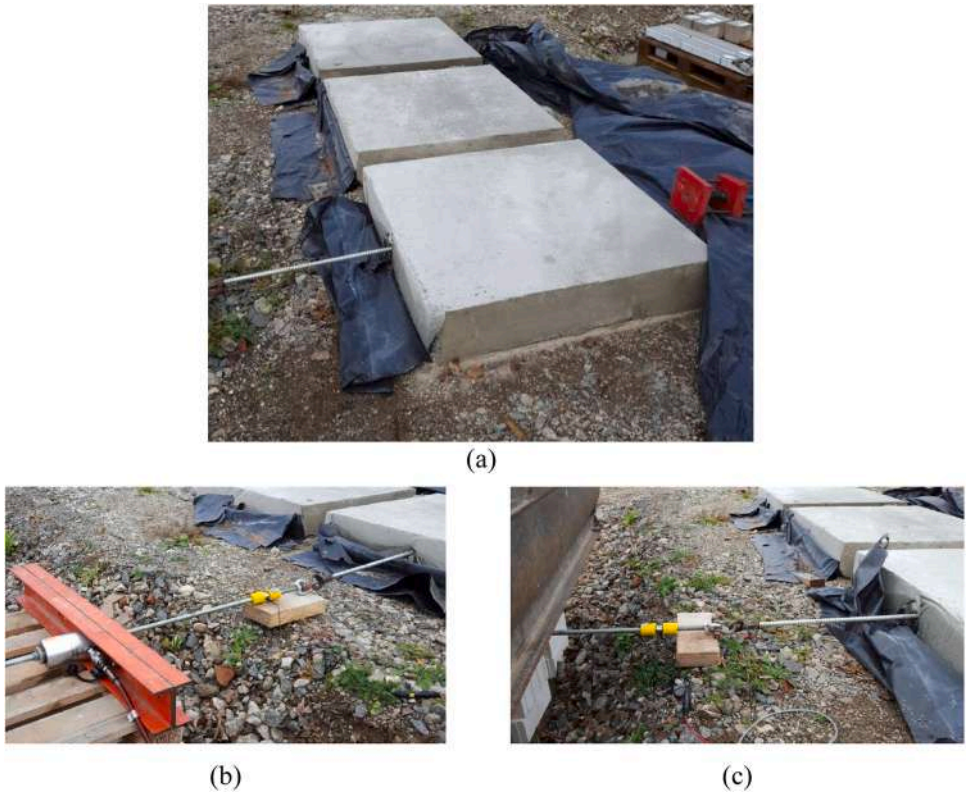

Fig. 6. Three square slab specimens before testing (a), hydraulic jack and a steel beam for applying in-plane horizontal load (b), anchoring system (c).

by the applied force assuming a uniform stress distribution on the contact surface) vs. slippage. A small scatter of results could be clearly pointed out and the corresponding mean experimental curve is also depicted (Fig. 7b); the maximum shear stress (average value) is equal to 0.0033 MPa at about 1 mm of slippage. In Fig. 7c, by adopting the approach proposed by Wimsatt et al. [31], a bilinear curve (dashed red line) is shown, whose parameters are: $\tau_0 = 0.0033$ MPa and $\delta_0 = 0.5$ mm; the latter parameters will be better described in Section 6 for applying a simplified analytical approach to predict the behavior of unidimensional slab. Moreover, in Fig. 7b the bilinear shear stresses vs. slippage laws proposed for natural clay and flexible granular subgrade [30,31] are also reported for the sake of comparison; it can be noticed that the use of double plastic sheet layer halves the friction occurring with respect to the lowest value available in literature.

4. Environmental conditions

Environmental temperature and relative humidity were measured continuously during the whole duration of the tests. Fig. 8a and b show the variations of temperature and relative humidity (RH) along the time of the tests, respectively. Since the slabs were located outside the laboratory, they were subjected to daily variations of temperature and relative humidity (RH); moreover, due to long term measurements, variations can be noted over the time, as well.

It can be noticed that, from 30 to about 40 days after casting, problems occurred in the recording process. In Fig. 8a, the mean daily

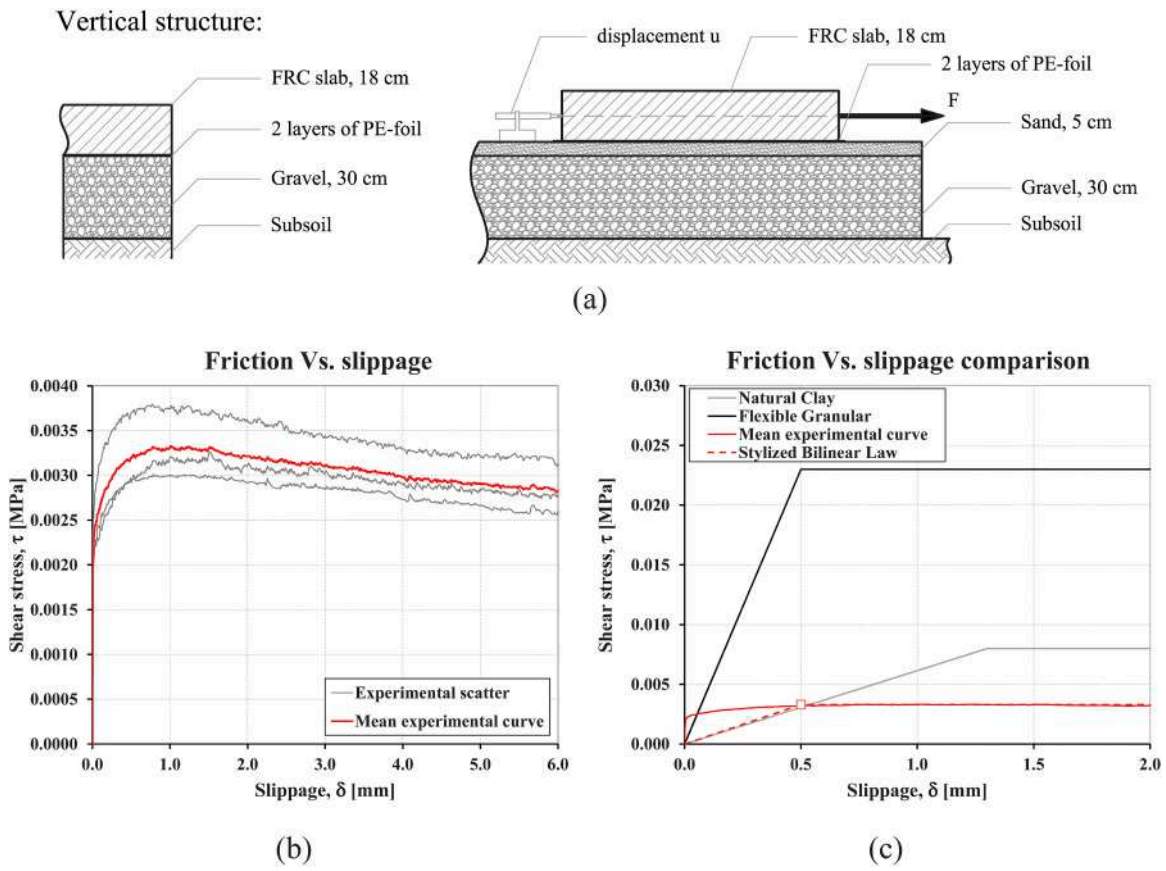

Fig. 7. Interfacial friction between slab and subgrade: test setup (a), friction vs. slippage behavior retrieved from three square slab specimens (b), stylized bilinear law derived (c).

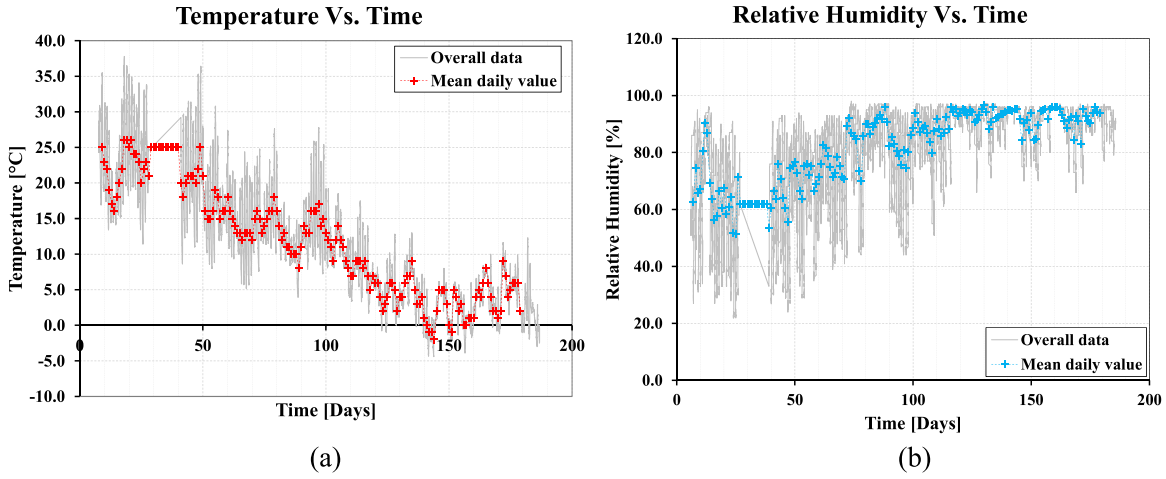

Fig. 8. Temperature (a) and relative humidity (b) of the environment vs. Time.

temperature (in red) decreases from 25 °C to around 0 °C with a maximum decrease of 30 °C, while Fig. 8b shows the relative humidity (mean daily value in light blue) that increased up to 95%.

5. Slabs instrumentation

Fig. 9a and b show the entire arrangement adopted for monitoring the square and unidimensional slab, respectively. Readings were collected through a data logger placed between the slabs. Because of the long period measurement, a continuum power supply was guaranteed to the data collection points to avoid data loss. A data recording frequency equal to 1/600 Hz (i.e. 1 data point every 10 min) was set.

The following transducers were adopted (Fig. 9a and b):

- 20 embedded Vibrating Wire Strain gauges type sensor in positions: 3, 4, 5, 8, 10, 11, 12, 13, 14, 15 to measure concrete deformation in terms of microstrains at two different slab's depths for each position (Fig. 10a);

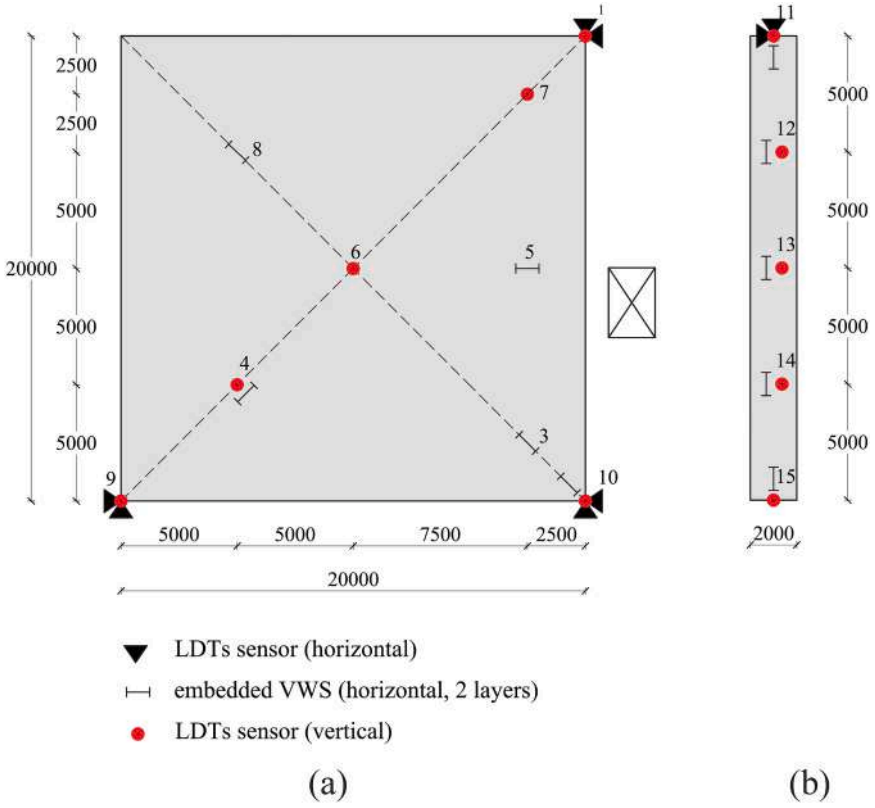

Fig. 9. Slabs' instrumentation: square slab (a), unidimensional slab (b) (dimensions in mm).

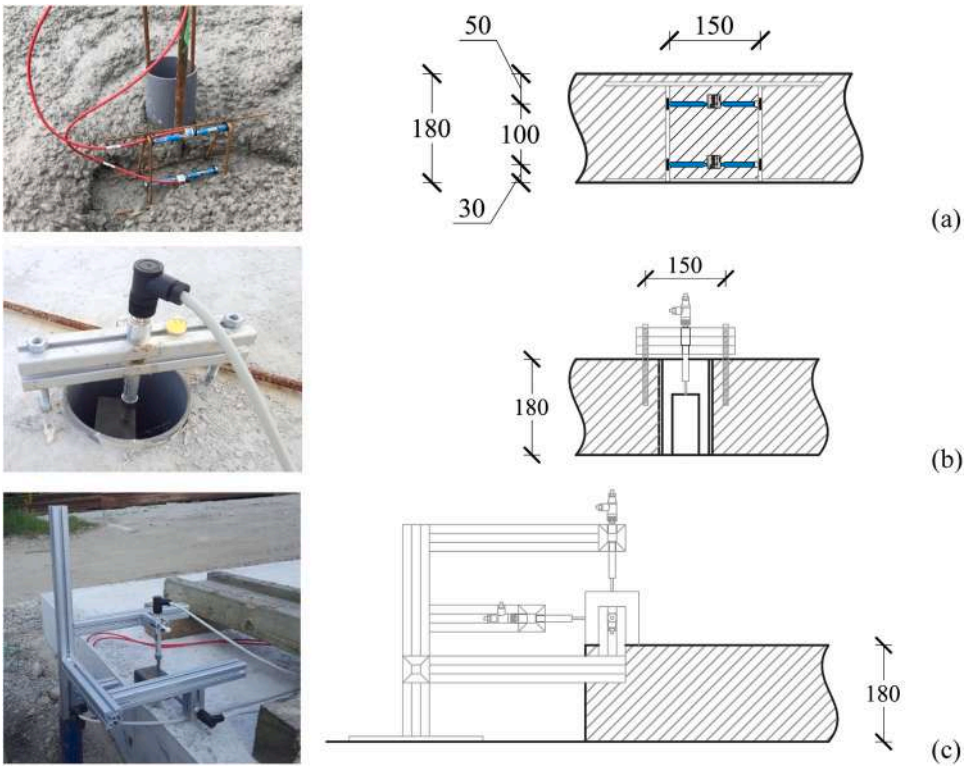

Fig. 10. Slabs' instrumentation details: embedded vibrating wire strain gauges (a), LDT inside slab perimeter for vertical displacement (b), LDTs at slab's corner/edge for displacements in three directions (c) (dimensions in mm).

- 8 Linear Displacement Transducers (LDTs) to detect horizontal in-plane-slab displacements (mm) in positions: 1, 9, 10, 11 (black triangles are depicted to evidence the directions of measurement);
- 11 Linear Displacement Transducers (LDTs) to measure vertical out-plane-slab displacements (mm) in positions: 1, 4, 6, 7, 9, 10, 11, 12, 13, 14, 15, shown with red dots.

Consequently, it is worth noticing that, at three corners of square slab (Fig. 9a) and at one edge of unidimensional slab (Fig. 9b), corresponding to data positions 1, 9, 10 and 11, respectively, the displacements in three directions were measured.

The concrete embedded vibrating wire strain gages (Model 4200 by Geokon), have an active nominal gage length of 153 mm. In order to measure the shrinkage development over the slab thickness, for each detection point, two sensors were arranged at 30 mm and 130 mm from slab bottom surface and kept in place by spacers (Fig. 10a).

The Linear Displacement Transducers (LDT, Model RP13/25-T-ST85 by TWK Elektronik), have a measuring stroke of 25 mm and a spring return for guaranteeing the perfect functioning along the entire measuring stroke range. LDTs were placed after casting by using specific arrangements reported in Fig. 10b and Fig. 10c. In Fig. 10b the sensor was clamped in an aluminum rod, which was anchored to the slab through dowels (before casting, a plastic pipe together with a spacer were positioned to create a hollow; Fig. 10b). During the test, LDT's moved together with the vertical slab displacement of detection points located inside the slab perimeters (n. 4, 6, 7, 12, 13, 14, 15 in Fig. 9a and b). Fig. 10c shows the device made of rods arranged to properly position three LDTs at slabs' corner/edge (n. 1, 9, 10 and 11 in Fig. 9a and b); thus, two in-plane displacements along two principal slab axis and a vertical displacement could be measured.

During the test, visual inspections of the slabs were scheduled to verify possible cracking phenomena on visible top surface.

6. Results

On the basis of visual inspections, both slabs remained free of cracks during the monitoring period (Fig. 11). This was probably possible because of the efficiency of glass macro-fiber to control cracking since very early ages as well as the initial curing period (Section 3.1), the environmental conditions (Section 4), and the reduced friction under the slab provided by the double sheet plastic layer (Section 3.2). These factors influence the behavior of the slab and its deformations, which result from the combination of the in-plane and out-plane displacements. Both types of displacements were measured by the instrumentation described in Section 5.

A significant data processing effort was required to obtain readable results because of the long-term monitoring and the consequent data complexity. The total amount of readings was filtered by considering different parameters (e.g.: time, temperature) depending on phenomena under investigation.

Fig. 11. Unidimensional slab (a) and square slab (b) at the end of monitoring period.

Fig. 12a and b provide a general overview of the vertical displacement for unidimensional slab and square slab, respectively. Light gray curves refer to the raw experimental data versus time. Based on sampling rate adopted (1/600 Hz), the full data set of one day is composed by 144 data for each sensor. For the sake of clearness, to obtain the daily vertical displacements, without expected daily fluctuations, a moving average procedure was applied as well. The moving average elements were determined by calculating the average of the data subset across consecutive days. Thus, the thicker colored continues lines plotted in Fig. 12a and b, stands for the average daily vertical displacements at the colored dot on the slabs.

Both slabs show a similar trend: after an initial settlement stage in which slabs sink and settle on the subgrade because of the dead weight, the free slab corners (red and black dots) start to uplift, presenting the well-known phenomenon of "upward curling" [19,20]; on the contrary, the central displacements (in light blue lines) remained nearly zero.

Moreover, the vertical uplift tends to increase more rapidly in the initial 50 days after which the displacement rate remarkably reduces. Based on the slab dimensions, the vertical uplift is rather low for both slabs. In the case of unidimensional slab, the maximum value is about 0.73 mm (at about 170 days) with respect to a half slab length of 20 m, which means that the corresponding curvature is rather limited (Fig. 12a). The same tendency can be clearly pointed out for square slab (Fig. 12b).

Considering the data collection points P11 vs. P15 (edges) and P12 vs. P14 (central point of half portion) of unidimensional slab (Fig. 12a), it can be noticed that the deformed shape is not symmetrical. Nevertheless, the same trend occurs for square slab (Fig. 12b), which would prove the reliability of readings. In fact, both lower half slabs are characterized by a higher corner uplift (points: P9, P10, P15) and a deeper sinking at a distance of about 5 m from the free slab side (points: P14 and P4); this behavior could be due to a slightly different subgrade settlement.

Vertical slabs' displacements shown in Fig. 12 could be affected by several environmental factors like temperature which may play a role on the concrete shrinkage. To better understand the "upward curling" phenomenon, the data of vertical displacements were further filtered by considering a given daily range of temperature. It was chosen a reference daily temperature-range of 14–18 °C, which is meaningful and representative of a wide range of days (up to 114 days). The aim is to focus the attention on the slabs deformations mainly governed by shrinkage effects. Fig. 13a and b plot the vertical displacement vs. time for the evidenced range of temperatures for unidimensional and square slab, respectively. The environment relative humidity variation over time is reported as well, based on data collected in Section 4. The general trends previously exhibited in Fig. 12 are confirmed; the entity of uplift displacements is also similar (at 114 days the difference is about 16% for unidimensional slab and 13% for square one), confirming that the shrinkage deformation has probably mainly governed the slabs' uplift and curling phenomena. Considering a fixed daily temperature range, the influence of only relativity humidity (RH) on the vertical slabs displacements was assessed in Fig. 13, excluding thermal effects. Hence the aim was to identify a nearly constant temperature range in which relative humidity varied significantly. The temperature range of 14–18 °C was chosen; based on the absolute extreme values of temperature (i.e. minimum and maximum values of about 0 °C and 35 °C, respectively) over the monitoring-time, the selected range represents the average temperature. Noteworthy is that this range has permitted to collect abundant data which well covered the monitoring-time of about 186 days in spite of the passing through different seasons resulting in a statistically representative subset of data.

For the investigated daily temperature-range, the RH is decreasing, and the shrinkage effects are amplified, even though, in absolute term, they are not so high (see Fig. 5a, Section 4) because the overall season temperature was reducing.

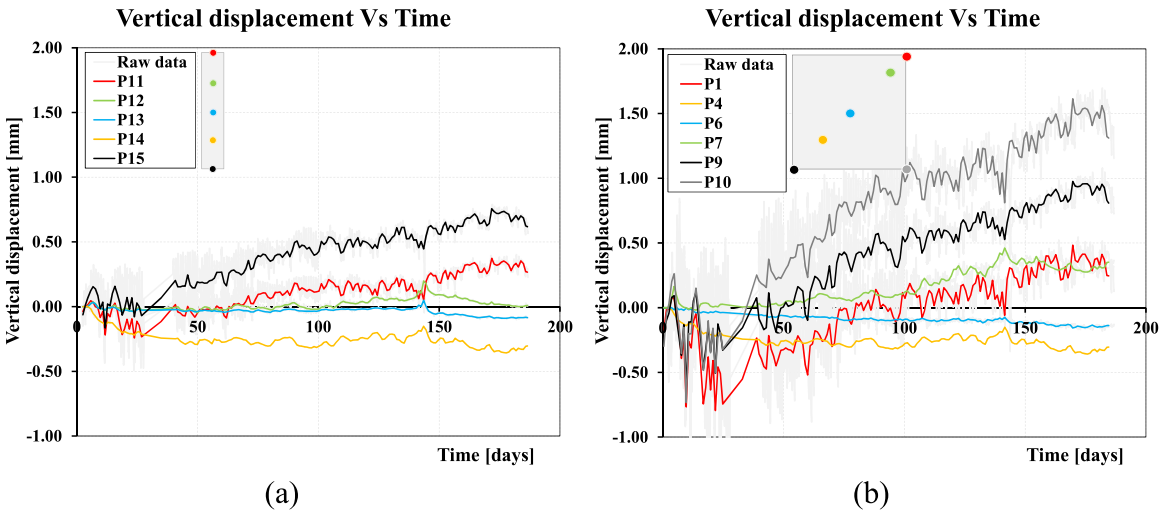

Fig. 12. Vertical displacement vs. Time retrieved from unidimensional slab (a) and from square slab (b).

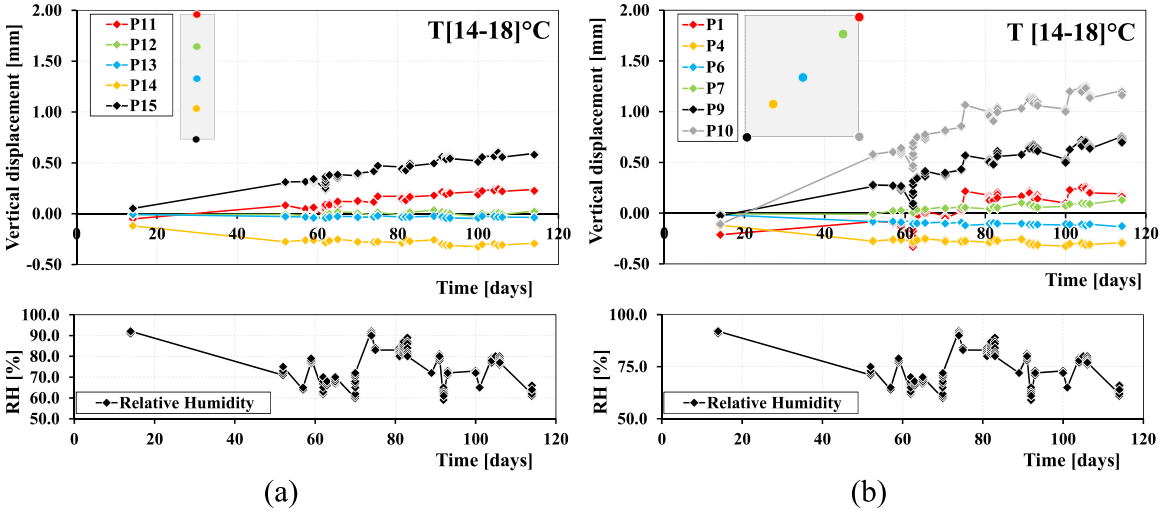

Fig. 13. Vertical displacement and Relative Humidity vs. Time filtered by temperature range (14–18 °C) for unidimensional slab (a) and for square slab (b).

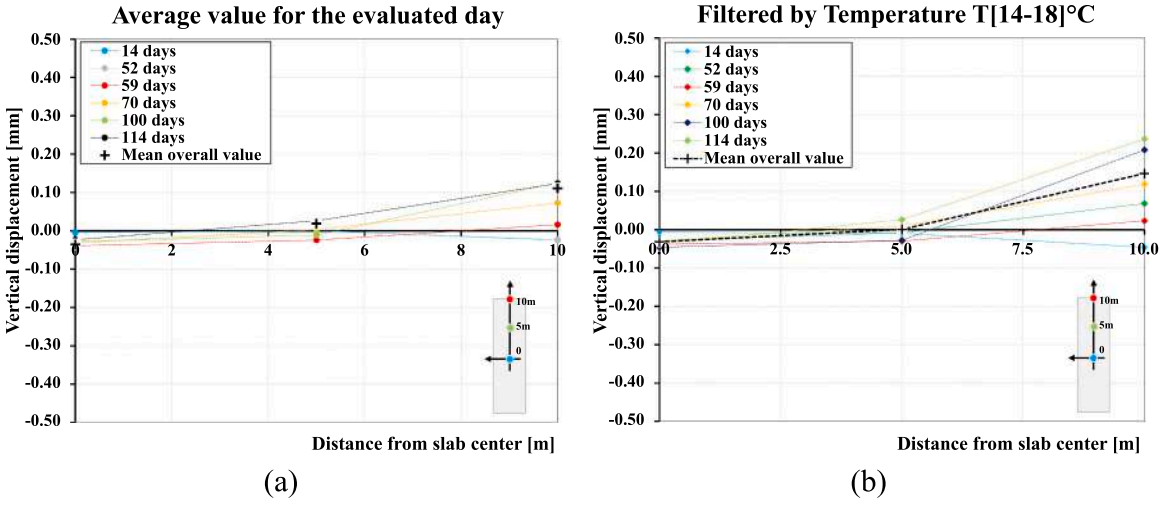

Fig. 14. Unidimensional slab: deformed shape along time by filtering by evaluated day (a) and by temperature (b).

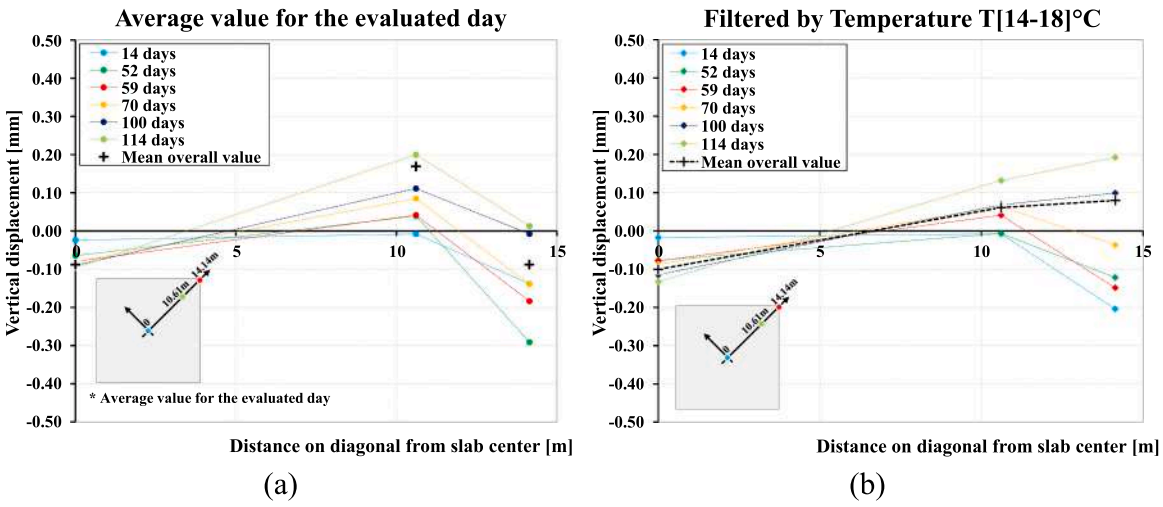

Fig. 15. Square slab: deformed shape along time for the evaluated day (a) and filtered by temperature (b).

Spatial distribution of out-plane slabs vertical displacements was also investigated by considering the distance from the center of the slabs measured along the longitudinal axis of unidimensional slab (Fig. 14) and diagonal of square slab (Fig. 15). Based on previous remarks concerning slabs non-symmetrical behavior, data for only half slabs are plotted (upper portions). Fig. 14a and Fig. 15a represent the average daily displacements, including both temperature and shrinkage effects; on the contrary, in Figs. 14b and 15b, displacements were filtered for a given range temperature (14–18 °C). The same reference days were adopted to get a direct comparison.

It can be noticed a different behavior between unidimensional slab and square slab. For the former, the edge at 10 m from the center progressively uplifts after 52 days until reaching a displacement of about 0.24 mm at 114 days for the given temperature (Fig. 14b). Moreover, it could be also noted that the central slab portion (4 m long from the center) remains in contact with the subgrade, making possible the constrained shrinkage due to friction.

As far as square slab is concerned, slab remains in contact with the subgrade for 14 days, with the end part settled down (Fig. 15a). Thereafter, at about 10.61 m from the center the slab tends to progressively lift up, even though the corresponding free corner always exhibit downward displacement (Fig. 15a). This could be related to the effect of downward slab-dead-weight acting on the uplifted portion but this tendency disappears in Fig. 15b. It can be derived that, probably, the daily temperature variation has more affected the deformed shape of the latter portion of square slab (Fig. 15a) while, when filtering temperature effects, the deflected shape presents free corners moving upward (Fig. 15b). In the latter case, the maximum upward corner displacement is 0.19 mm at 114 days for the given temperature (Fig. 15b), which is similar to 0.24 mm edge displacement shown in Fig. 14b for unidimensional slab, even though the reference length from the center is different: 10 m and about 14 m for unidimensional and square slab, respectively (as schematically depicted in Figs. 14b and 15b). Nevertheless, it is worth noting that both are rather low values, confirming that only minor induced curling effects were evidenced.

The in-plane slabs behavior was also investigated. In Fig. 16a the time development of displacements detected at points P11 and P15 of unidimensional slab are reported together with the corresponding slab global shortening (thicker black line), which progressively increase up to about 7.2 mm after 184 days. Regarding square slab, a similar trend can be appreciated in Fig. 16b, where the displacements detected at points P1, P9, P10 were combined to get the in-plane displacements along slab's diagonals. Considering measurements detected at P1 vs. those occurred at P9 and P10, it can be noticed almost a symmetrical behavior of the upper slab portion with respect to the bottom one. Along the diagonal defined by points P1 and P9, the slab shortening was also estimated, whose maximum value is about 10.9 mm after 184 days, which is about 50% higher than that exhibited by unidimensional slab.

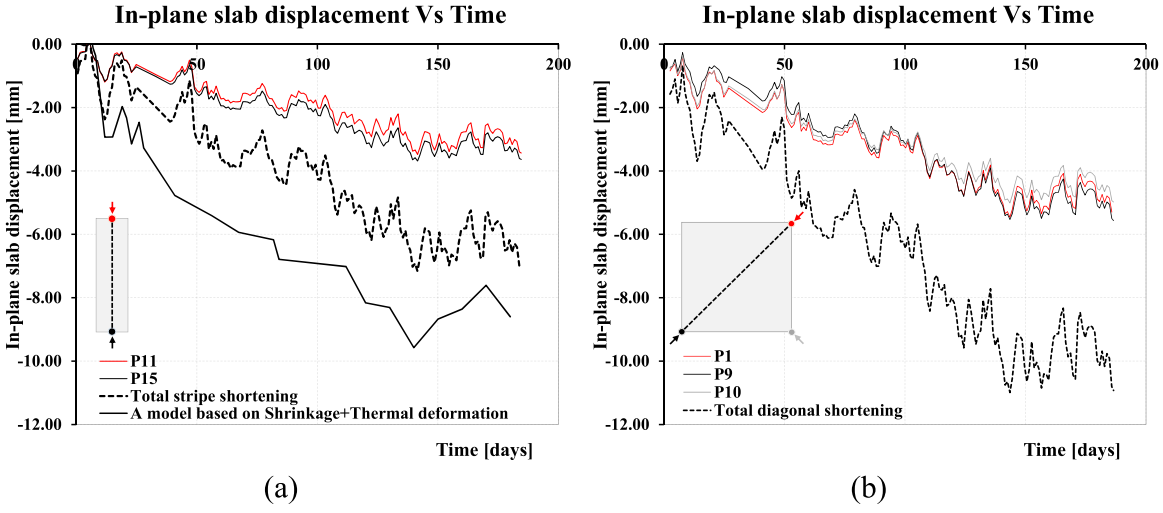

Fig. 16. In-plane slabs displacement vs. Time: unidimensional slab (a), square slab (b).

This trend can be mainly related to the diagonal length of the square slab (about 28 m), which is about 40% longer than the 20 m length of unidimensional slab.

Based on LDTs measurements previously reported, the fields of deformations occurring in slabs are mainly governed by in-plane behavior rather than out-plane one, induced by bending. To better study these aspects, readings of embedded vibrating wire sensors were elaborated: the mean value of the measurements exhibited by two adopted layers (Fig. 10a) is considered for describing the in-plane deformation (Fig. 17), while the corresponding gradient is evaluated for determining the curvature (Fig. 18). In both cases, the time evolution is presented for all data collection points.

Fig. 17 shows the in-plane slab deformations which tend to raise slightly over the time. The deformations recorded by strain gauges include shrinkage and thermal effects being superimposed to concrete deformations related to stresses. Thus, the compressive strains recorded by sensors (positive ordinate in Fig. 17) are in agreement with shrinkage and the progressive season temperature decrease. In some data collection points of unidimensional slab (e.g.: P15 in Fig. 17a) and of square slab (e.g.: P5 in Fig. 17b), the strains are rather low, probably as result of difficult readings by embedded sensors.

Based on the in-time development of curvature in section under investigation, both the unidimensional slab (Fig. 18a) and the square one (Fig. 18b) exhibit negligible induced flexural phenomena as result of limited strain gradient detected along the thickness. Hence, an in-plane shortening mainly occurs (Fig. 17) and this tendency is in agreement with limited curling phenomenon evidenced by vertical displacements transducers (Fig. 14 and Fig. 15).

The unidimensional slab experimentally tested can be schematized, as a first approximation, as a simplified ideal beam element on continuum subbase. Moreover, it remains un-cracked and it has been proven that the deformed shape is mainly governed by in-plane shortening with almost negligible flexural behavior. Accordingly, the simplified analytical model proposed by Zhang et al. [23,24] can be reasonably applied for predicting slab behavior, since the approach considers a linear elastic concrete beam on subbase subjected to uniform in-plane deformation only. Moreover, in this model the frictional behavior between the beam and subbase is described by means of a bi-linear law for which experimentally determined parameters shown in Fig. 7c can be adopted (τ_0 =0.0033 MPa and δ_0 =0.5 mm). Concrete elastic modulus (E_c) can be introduced as a time-dependent input parameter based on Fig. 3c, together with the total imposed deformation (main input-data). The latter is calculated by summing the free-shrinkage deformation retrieved from prisms under on-site conditions (Fig. 5a) and thermal strain which can be evaluated by assuming the thermal expansion concrete coefficient equal to 10^{-5}/°C as well as the measured environmental temperature development (Fig. 8a), even though it does not exactly correspond to temperature exhibited inside the slab.

Within the aforementioned hypotheses, the predicted in-plane shortening time development of unidimensional slab is plotted in Fig. 16a and compared to experimental results: a general good agreement can be noticed, even though the approach proposed by Zhang et al. [23,24] overestimates the experimental value of about 30%; this could be related to the conservative temperatures assumed in the slab and the simplified frictional law adopted.

7. Concluding remarks

The shrinkage and thermal deformation behavior of Glass-FRC slabs-on-grade in outdoor conditions was investigated in this study by means of real-scale experimental tests that involved a complete monitoring during a period of about six months. The time development of main Glass-FRC mechanical properties as well as environmental conditions were measured together with a continuous recording of in-plane and out-plane slab displacements, and deformations over the slab thickness.

Based on the results of the present study, the following conclusions can be drawn:

1. The glass macro-fiber reinforcement used in the 20×20 m slab-on-grade can be an efficient solution to control cracking from shrinkage and thermal deformations and, through visual observations after approximately 6 months, no cracks appeared on the slab surface.
2. The slab-to-support friction was studied through large experimental tests; the response shows a rise-constant behavior with a maximum friction or shear stress of 0.0033 MPa when two layers of plastic sheet are interposed between the slab and the ground.
3. The slab behavior is mainly governed by in-plane deformations, as proven by displacement sensors and confirmed by embedded vibrating wire strain gauges.
4. Only minor induced curvature or curling was evidenced through the measures of the implemented instrumentation, even with the testing time occurring through a significant part of the European summer.
5. In the case of the un-cracked unidimensional slab mainly governed by in-plane behavior, it is possible to predict the in-plane experimental displacements through a simplified analytical model available in literature with a rather good agreement taking advantage of the governing parameters measured experimentally.

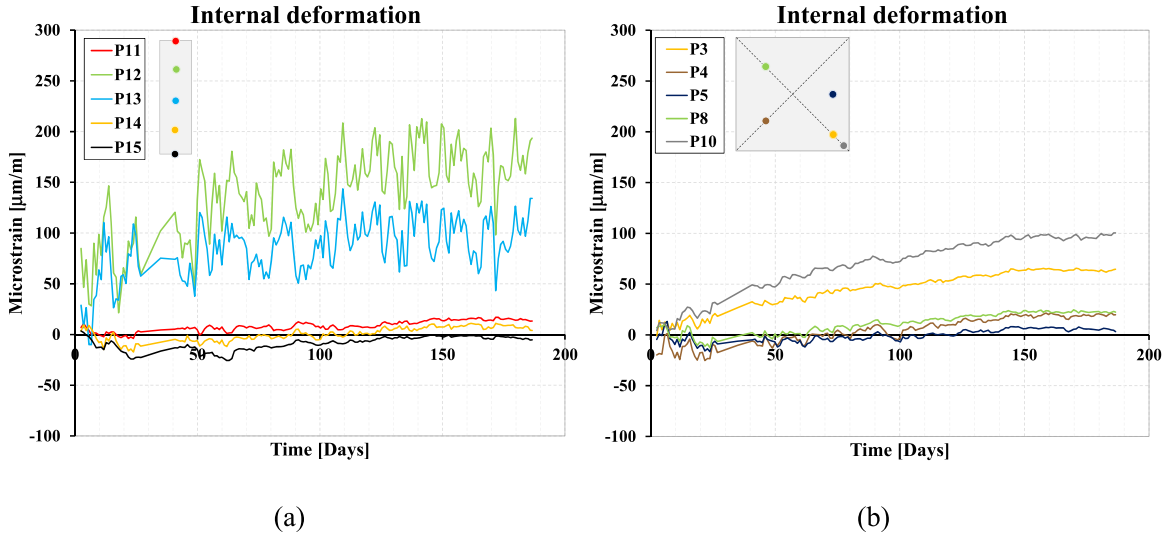

Fig. 17. Internal in-plane slab deformation vs. Time for unidimensional slab (a) and for square slab (b).

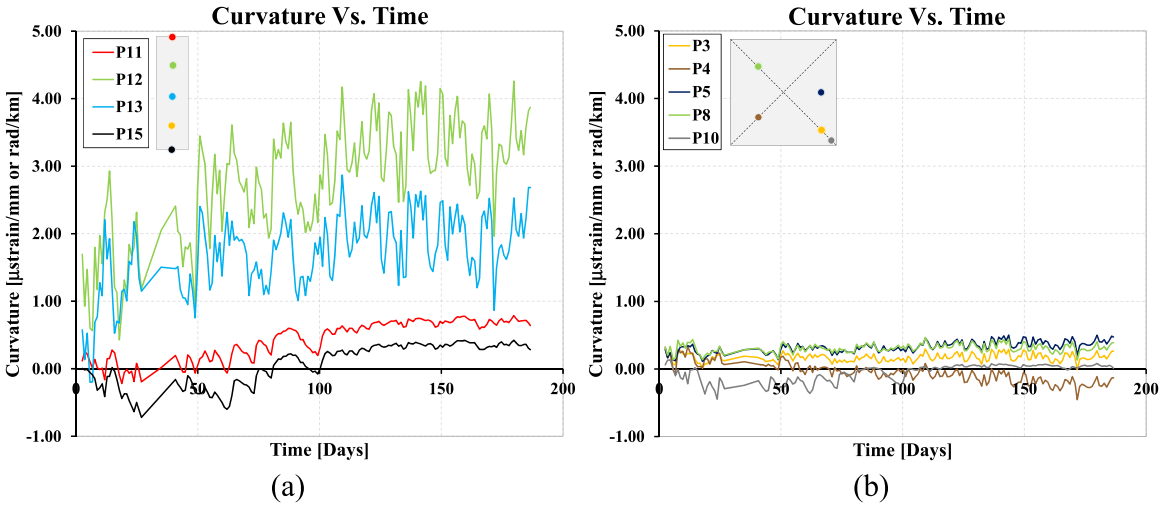

Fig. 18. Curvature vs. Time for unidimensional slab (a) and for square slab (b).

CRediT authorship contribution statement

Barragan Bryan: Writing – review & editing. **Tiberti Giuseppe:** Writing – review & editing, Project administration, Methodology, Data curation, Conceptualization. **Löber Philipp:** Investigation, Conceptualization. **Holschemacher Klaus:** Supervision, Conceptualization. **Friedemann Stephan:** Supervision, Resources. **Plizzari Giovanni:** Supervision, Resources, Project administration. **Mudadu Antonio:** Writing – review & editing, Writing – original draft, Data curation.

Declaration of Competing Interest

The authors declare that they have no known competing financial interests or personal relationships that could have appeared to influence the work reported in this paper.

Data availability

Data will be made available on request.

Acknowledgments

The Authors are thankful to eng. Martin Willno for the support in monitoring and initial elaboration of data. A special acknowledgment goes to the construction company OTTO HEIL GmbH & Co. KG for providing the place, materials and assistance for casting and monitoring these full-scale slab samples.

References

[1] ACI 302.1R. Guide for Concrete Floor and Slab Construction; Technical Documents; 1996, p. 65.
[2] ACI 360 R-92. Design of Slabs on Grade; Technical Documents, 1997, p. 57.
[3] CNR DT-211. Istruzioni per la progettazione, l'esecuzione ed il controllo delle pavimentazioni di calcestruzzo; Consiglio Nazionale delle Ricerche; 2014, p. 104.
[4] British Concrete Society. Concrete Industrial Ground Floors: A Guide to Design and Construction, Technical Report No. 34, 3rd Edition; 2003, p 140.
[5] Timoshenko S., Woinowsky-Krieger S. Theory of plates and shells. ISBN 0–07-064779–8; 1987, p 580.
[6] Meda A, Plizzari GA. New design approach for steel fiber-reinforced concrete slabs-on-ground based on fracture mechanics. ACI Struct J 2004;101(3):298–303.
[7] Sorelli LG, Meda A, Plizzari GA. Steel fiber concrete slabs on ground: a structural matter. ACI Struct J 2006;103(4):551–8.
[8] Falkner H, Huang Z, Teutsch M. Comparative study of plain and steel fiber-reinforced: concrete ground slabs. Concr Int 1995;17(1):45–51.
[9] Tatnall PC, Kuitenbouwer L. Steel fiber reinforced concrete in industrial floors. Concr Int 1992;14(12):43–7.
[10] Aidarov S, Mena F, de la Fuente A. Structural response of a fibre reinforced concrete pile-supported flat slab: full-scale test (art. no) Eng Struct 2021;239: 112292. https://doi.org/10.1016/j.engstruct.2021.112292.
[11] Vasanelli E, Micelli F, Aiello MA, Plizzari G. Long term behavior of FRC flexural beams under sustained load. Eng Struct 2013;56:1858–67. https://doi.org/10.1016/j.engstruct.2013.07.035.
[12] Nogales A, de la Fuente A. Numerical-aided flexural-based design of fibre reinforced concrete column-supported flat slabs (art. no) Eng Struct 2021;232: 111745. https://doi.org/10.1016/j.engstruct.2020.111745.
[13] Leporace-Guimil B, Mudadu A, Conforti A, Plizzari GA. Influence of fiber orientation and structural-integrity reinforcement on the flexural behavior of elevated slabs (art. no) Eng Struct 2022;252:113583. https://doi.org/10.1016/j.engstruct.2021.113583.
[14] Conforti A, Cuenca E, Zerbino R, Plizzari GA. Influence of fiber orientation on the behavior of fiber reinforced concrete slabs. Struct Concr 2021;22(3):1831–44. https://doi.org/10.1002/suco.202000612.
[15] Germano F, Tiberti G, Plizzari G. Post-peak fatigue performance of steel fiber reinforced concrete under flexure. Mater Struct 2016;49(10):4229–45. https://doi.org/10.1617/s11527-015-0783-3.
[16] Nayar SK, Gettu R. A comprehensive methodology for the design of fibre reinforced concrete pavements. SP 310. ACI Special Pubblication; 2014. p. 321–30. SP 310.
[17] Barragán B., Facconi L., Laurence O., Plizzari G. Design of glass-fibre-reinforced concrete floors according to the fib Model Code 2010, American Concrete Institute, ACI Special Publication; 2014-July (SP 310), pp. 311–320.
[18] Tiberti G, Mudadu A, Barragan B, Plizzari G. Shrinkage cracking of concrete slabs-on-grade: a numerical parametric study. Fibers 2018;6(3). ISSN: 2079-6439, doi: https:/doi.org/10.3390/fib6030064.
[19] Suprenant BA. Why slabs curl part I: a look at the curling mechanism and the effect of moisture and shrinkage gradients on the amount of curling. ACI Concr Int 2002; 24(3):56–61.
[20] Suprenant BA. Why slabs curl part II: factors affecting the amount of curling. ACI Concr Int Farming Hill 2002;24(4):59–61.
[21] Ytterberg RF. Control of shrinkage and curling in slabs on grade Part I: shrinkage problems: causes and cures. Concr Constr 1992:5.
[22] Ytterberg RF. Control of shrinkage and curling in slabs on grade Part II: How to deal with warping and curling. Concr Constr 1992:5.
[23] Zhang J, Leng B. Analysis of shrinkage-induced stresses in concrete pavements. 2004 Mag Concr Res 2004;56(10):585–95. https://doi.org/10.1680/macr.2004.56.10.585.
[24] Zhang J, Li V. Influence of supporting base characteristics on shrinkage-induced stresses in concrete pavements. J Transp Eng 2001;127(6):455–62.
[25] Banthia N, Bindiganavile V, Azhari F, Zanotti C. Curling control in concrete slabs using fiber reinforcement. J Test Eval 2014;42(2):18. https://doi.org/10.1520/jte20120111.
[26] Reggia A, Tortelli S, Marchi M, Borsa M, Plizzari GA. Analysis of a jointless floor with calcium sulpho-aluminate and portland cement. ACI Special Publication. SP 2015;305:45.1–45.10.
[27] Garber G. Concrete floors: design and construction of concrete floors. 2nd edition.,. Butterworth-Heinemann, Elsevier,; 2006. p. 384.
[28] Neal FR. Concrete industrial ground floors: ICE design and practice guide. 2nd edition.,. Heron Quay, London: Thomas Telford Publishing; 2002. p. 62.
[29] Shadravan S, Ramseyer C, Kang TH-K. A long term restrained shrinkage study of concrete slabs on ground. Eng Struct 2015;102:258–65. https://doi.org/10.1016/j.engstruct.2015.08.018.
[30] Wesevich J.W., McCullough B.F., Burns N.H. Stabilized subbase friction study for concrete pavements. Res. Rep. 495–1, Ctr. for Transp. Res., University of Texas at Austin, Austin, Texas; 1987, p. 182.

[31] Wimsatt A.W., McCullough B.F., Burns N.H. Methods of analyzing and factors influencing frictional effects of subbases. Res. Rep. 495–2F, Ctr. for Transp. Res., University of Texas at Austin, Austin, Texas; 1978, p. 77.
[32] Facconi L, Minelli F, Plizzari G. Steel fiber reinforced self-compacting concrete thin slabs – experimental study and verification against model code 2010 provisions. Eng Struct 2016;122:226–37. https://doi.org/10.1016/j.engstruct.2016.04.030.
[33] Barragán B, Mudadu A, Tiberti G, Plizzari G. GFRP Reinforced concrete slabs under restrained shrinkage. Concr Int 2023;45(7):39–45.
[34] EN 12390–3, CEN European Committee for Standardization. Testing hardened concrete – Part 3: Compressive strength of test specimens; 2003, p. 20.
[35] EN 12390–6, CEN European Committee for Standardization. Testing hardened concrete – Part 6: Tensile splitting strength of test specimens; 2010, p. 14.
[36] EN 14651. Test method for metallic fibre concrete – measuring the flexural tensile strength (limit of proportionally (LOP), residual), European Committee for Standardization; 2005, p. 18.
[37] EN 12390–16. Testing hardened concrete - Part 16: Determination of the shrinkage of concrete; 2019, p. 13.
[38] EN 12350–5:2009 - Testing fresh concrete - Part 5: Flow table test.
[39] EN 1992–1-1. Eurocode 2: design of concrete structures – Part 1: general rules and rules for buildings; European Committee for Standardization; 2004, p. 225.
[40] Holschemacher K., Löber P. Experimental investigation on friction between foundation slabs and substructure. In Proc. of 13th International Conference of Modern building materials, structures and techniques, Vilnius, Lithuania; 16–17 May 2019, Vilnius Gediminas Technical University, DOI: https:/doi.org/10.3846/mbmst.2019.143.